Isotopic substitution reveals the importance of aluminate diffusion dynamics in gibbsite ($Al(OH)_3$) crystallization from alkaline aqueous solution

Anthony J. Krzysko[a,*], Trent R. Graham[b], Mateusz Dembowski[c], Chelsie Beck[b,d], Xin Zhang[b], Kevin M. Rosso[b], Sue B. Clark[b,d], Carolyn I. Pearce[b,e]

[a] Structural Sciences, Argonne National Laboratory, Lemont, IL 60439, United States
[b] Pacific Northwest National Laboratory, Richland, WA 99354, United States
[c] Los Alamos National Laboratory, Los Alamos, NM 87545, United States
[d] Department of Chemistry, Washington State University, Pullman, WA 99164, United States
[e] Department of Crop & Soil Sciences, Washington State University, Pullman, WA 99164, United States

[*]Corresponding author, Anthony.Krzysko@anl.gov

Abstract

Understanding molecular-scale factors governing the precipitation of aluminum hydroxides, such as gibbsite, under alkaline conditions is important for the formation of laterite deposits, as well as aluminum processing. However, mechanisms enabling tetrahedral aluminate ions to assemble into octahedral sites of the gibbsite lattice remain unclear. Formation of oligomeric complexes has been hypothesized as a critical intermediate step. Here, we report a study of gibbsite solubility in highly alkaline solutions using deuterium substitution to probe equilibrium and kinetic factors that could affect oligomeric intermediate formation, including the reactivity and the diffusivity of aluminate ions. When substituting sodium hydroxide with sodium deuteroxide, solution analysis shows a nearly 40% and 50% increase in gibbsite solubility in 2.4 and 3.3 $mol \cdot kg^{-1}$ total sodium solutions, respectively. Raman spectroscopy indicated that monomeric aluminate ions are the predominant species in solution irrespective of deuteration. However, both ^{27}Al and ^{23}Na nuclear magnetic resonance (NMR) spectroscopy revealed significant differences in chemical shifts in deuterated solutions, and analysis of ^{1}H, ^{23}Na, and ^{27}Al diffusion coefficients with pulsed-field gradient, stimulated echo NMR spectroscopy shows a decrease in ion diffusivity with increasing total deuterium in solution, consistent with the notion of increasing strength in the hydrogen/deuterium bonding network. Because the relative change in ^{1}H diffusion coefficients are commensurate with the difference in apparent solubility constants, there is evidence for an oligomeric intermediate whose steady-state concentration is maintained by the collision frequency of aluminate ions.

Keywords

Gibbsite, aluminate, deuterium, isotopic substitution, solubility

1.0 Introduction

Classical crystal growth is characterized by the attachment of monomeric atoms, ions, or molecules onto a primary nucleus or crystal. However, non-classical mechanisms involving assembly from amorphous or cluster intermediates are increasingly recognized as critically important in nucleation, crystal growth, and precipitation.[1–5] This is especially true for reactions in non-ideal chemical conditions, such as in water-in-salt electrolytes where water activity is low and solvent species strongly influence the behavior of the system.[6,7] Given that there is evidence for cluster-based nucleation pathways, even at solution conditions thought to be ideal, non-ideality may be commonplace in crystal growth,[8] despite remaining poorly understood.[9] Furthermore, the solvent or background electrolytes (nominally called spectator ions) can affect reactions more than previously thought.[10]

The present study seeks to improve the fundamental understanding of nonclassical growth pathways that may underpin crystallization of gibbsite (α-$Al(OH)_3$). Gibbsite is a ubiquitous soil mineral, where it can act as an important sorbent of toxic or radioactive elements.[11–14] Gibbsite is also the dominant mineral in bauxite deposits, the major ore for aluminum (Al) production. Crystallization of gibbsite under alkaline conditions is relevant to bauxite formation from lateritic weathering of ultrabasic rock[15], bauxite processing via the Bayer process,[16] and for the processing of Cold War nuclear waste.[17–23] Under the current nuclear waste retrieval plan, gibbsite dissolution will be achieved using alkaline solutions with excess sodium hydroxide.

Under alkaline conditions, the relevant equilibrium determining gibbsite crystallization is given by (**Eq**. **1**).[24]

$$Al(OH)_3(s) + OH^-(aq) \rightleftharpoons Al(OH)_4^-(aq) \qquad (\mathbf{1})$$

Substantial research has been conducted on the energetics and kinetics of reaction (**1**), but many uncertainties remain.[25,26] For example, the experimentally determined solubility values for various aluminum (oxy)hydroxides exhibit wide and conflicting values.[27] Similarly, it is unclear whether gibbsite crystallizes directly from monomers of aluminate ions, or from oligomeric intermediates maintained at much lower concentration by rapid conversion to gibbsite. The ongoing ambiguities in possible solution

species and structure was highlighted in a review of results derived from a variety of experimental techniques including nuclear magnetic resonance (NMR) spectroscopy, X-ray scattering, and neutron scattering.[28] Of central importance is that the principally tetrahedral coordination of the aluminate ion is in contrast with the octahedral coordination of Al in gibbsite. A recent molecular dynamics simulation using umbrella sampling found stable intermediate coordination states of Al on gibbsite surfaces during dissolution at high pH,[29] and similarly there is evidence for under-coordinated Al on gibbsite synthesized from amorphous aluminum hydroxides under acidic conditions, possibly suggesting interface-mediated Al coordination changes.[30] Finding direct spectroscopic evidence of a reaction pathway bridging the discontinuous coordination between octahedral- and tetrahedral-coordinated aluminum remains an active area of research. Recently, in-situ ^{27}Al magic angle spinning NMR was used to study coordination changes during transformation of gibbsite or sodium aluminate hydrates; however, it was not possible to identify intermediate species within the timescale of the measurement at the system compositions of those studies.[31]

While the mechanism has not been directly observed, translational dynamics are implicitly important to crystallization if it involves aluminate monomers coming together to form oligomeric intermediates for precipitation to occur. Substitution of deuterium for protium leads to changes in chemical reactivity,[32] often due to changes in reaction kinetics,[33] that can be used to gain insight into mechanisms of both precipitation and dissolution.[34–37] In a prior study of supersaturated sodium aluminate solutions at elevated temperatures, deuteration was noted to cause a different $Al(OH)_3$ polymorph, bayerite (β-$Al(OH)_3$), to co-precipitate in the presence of gibbsite seeds.[38] However, there was no mention of bayerite formation in an additional scanning electron microscopy (SEM) study by the same group using similar conditions.[39] It was further speculated that differences in gibbsite morphology were due to differences in the hydrogen bonding of deuterated solutions. Specifically, it was noted that differences in hydrogen bond strength would affect the formation of clusters that are mechanistically important to gibbsite precipitation, although no spectroscopy on solution species was performed to quantify these differences. It was proposed that an increase in cluster formation in deuterated solutions would be expected due an increase in nucleation events. Although the effect of deuteration on the hydrogen bond network is complicated and can be system

specific,[33,40,41] these initial studies suggest that systematic analysis of the effects of deuterium-substitution could provide insights into factors controlling gibbsite crystallization in alkaline solutions.

Here, sodium hydroxide solutions that are substituted with deuterium to various extents are used to explore the isotope effect on gibbsite solubility, a phenomenon requiring both dissolution and precipitation reactions to reach equilibrium. A combination of inductively coupled plasma optical emission spectroscopy (ICP-OES), ^{23}Na and ^{27}Al NMR spectroscopy was used to quantify the reaction quotient for gibbsite solubility as a function of the amount of deuterium substitution for protium in solution. The speciation of Al in sodium hydroxide and deuteroxide solutions was then determined using ^{27}Al NMR and Raman spectroscopy. The effect of deuterium substitution on the strength of the hydrogen bonding network was quantified using ^{1}H, ^{23}Na, and ^{27}Al diffusion with pulsed field gradient, stimulated echo NMR spectroscopy. It is hypothesized that strengthening the hydrogen bonding network would cause a decrease in Al ion diffusion, which would lead to slower nucleation if it were predicated upon transient formation of oligomeric Al ion intermediates. We observed a decrease in the precipitation of gibbsite in deuterated sodium hydroxide, and an attendant increase in gibbsite solubility, consistent with this main hypothesis. This suggests an important governing role of transient oligomeric Al ion intermediates in the nucleation and growth of gibbsite in alkaline geochemical and artificial systems.

2.0 Experimental

2.1 Solubility experiments

All reagents and solubility experiments were prepared and performed in an argon-filled glovebox to limit the exposure of the sodium hydroxide (NaOH) solution to carbon dioxide. Gibbsite nanoplates were synthesized and characterized as described in the literature.[30,42] A representative pXRD pattern of the starting material and the expected pXRD pattern are shown in **Figure S.1**. Solubility experiments were performed at 2 different total sodium concentrations (nominally 2.4 and 3.3 mol·kg^{-1} total sodium), each experiment was performed in triplicate (3 experiments for each ratio of H:D). The concentration of total

sodium for each experiment at different timepoints was determined using ICP-OES and the triplicate results were averaged. The 2.4 ± 0.2 and 3.3 ± 0.1 mol·kg^{-1} stock NaOH solutions were made by diluting concentrated NaOH (50% wt, Sigma Aldrich, St. Louis, MO, USA) with deionized H_2O. The 2.4 ± 0.2 and 3.2 ± 0.1 mol·kg^{-1} stock NaOD solution were made by diluting NaOD (40% wt in D_2O, Sigma Aldrich) with D_2O (99.90%, Sigma Aldrich). The mixed deuterium and protium stock solutions were made by combing equal masses of the NaOH and NaOD solutions, resulting in solutions of 2.6 ± 0.1 and 3.3 ± 0.1 mol·kg^{-1}. Gibbsite was added to each experiment and the total amounts of gibbsite and solvent are shown in **Table 1**.

Table 1. The average amount ± 3 σ of each reagent used for the experiments performed in this study. The number of samples is 3 for each solution.

Experiment	Total Mass gibbsite (g)	NaOH solution (g)	NaOD solution (g)
2.4 mol·kg^{-1} NaOH	0.415 ± 0.007	7.97 ± 0.01	0
2.4 mol·kg^{-1} mixture	0.415 ± 0.004	3.96 ± 0.03	3.98 ± 0.03
2.4 mol·kg^{-1} NaOD	0.414 ± 0.005	0	7.99 ± 0.05
3.3 mol·kg^{-1} NaOH	0.950 ± 0.010	8.40 ± 0.04	0
3.3 mol·kg^{-1} mixture	0.948 ± 0.006	4.18 ± 0.03	4.24 ± 0.05
3.3 mol·kg^{-1} NaOD	0.948 ± 0.008	0	8.44 ± 0.08

Gibbsite dissolution was performed using the hydroxide and deuteroxide stock solutions described above. Each experiment was performed in triplicate, with a reagent blank that did not contain gibbsite. The solutions bearing gibbsite powder were shaken in a glovebox simultaneously so that the temperature was consistent for each experiment (≈ 300 K). The total aluminum and sodium concentrations for each time point were determined by centrifuging the samples (500 rpm for 10 min in the same 20 mL LSC vials where the reaction occurred to allow for solid settling), submitting small aliquots (15 µl, to reduce the total volume change in the experiment) to ICP-OES, and averaging the results for each condition (n = 3). The masses of each aliquot were determined prior to ICP-OES analysis for molality calculations. In addition, aliquots from the solutions at equilibrium were analyzed using ^{27}Al and ^{23}Na NMR.

The effect of deuterium on the solid phase was investigated by washing the residual solids (× 3) with the appropriate water (either H_2O, H_2O + D_2O mixture, or D_2O), drying overnight (310 K), and then

conducting pXRD analysis. Additional unwashed residual solids were dried (310 K) and analyzed by pXRD. Because the unwashed solids were found to contain bayerite, an additional experiment was performed to investigate the effects of leaving gibbsite in a saturated solution with residual molar amounts of NaOH. Gibbsite was dissolved in various volumes of the stock 2.4 $mol \cdot kg^{-1}$ NaOH solution so that the residual molar ratios (NaOH : gibbsite) were ≈ 2, 4, 5, and 7. The solids were not washed with H_2O, but were dried (310 K for 24 h) and analyzed by pXRD.

2.2 Inductively coupled plasma-optical emission (ICP-OES)

For the 2.4 $mol \cdot kg^{-1}$ data set, concentrations of Al and Na were obtained using a PerkinElmer Optima 8300 dual view ICP-OES spectrometer (PerkinElmer, Waltham, MA) with a PerkinElmer S-10 auto-sampler interface. Calibrations were performed using standards (High-Purity Standards Corporation, Charleston, SC) ranging from 50 ppb to 50 ppm. The calibration was verified using an initial and continuing calibration verification, which was performed every 10 samples.

For the 3.3 $mol \cdot kg^{-1}$ data set, concentrations Al and Na were obtained using a Thermo iCAP7600 ICP-OES Duo (Thermo Scientific, Waltham, MA) equipped with standard quartz sample introduction. The instrument was calibrated using dilutions of 1000 ppm single element standards from Inorganic Ventures (Christiansburg, VA) in 2% HNO_3. Multiple wavelengths of aluminum and sodium were selected and compared to identify interferences. Check solutions were made with a similar ratio of Na:Al as the samples and analyzed every 10 samples to evaluate instrument precision and calibration accuracy.

2.4 Powder X-ray diffraction (pXRD)

pXRD patterns were collected on a Phillips diffractometer equipped with a graphite post-diffraction monochromator and a CuKa X-ray source (λ = 1.5406 Å). Samples were loaded into zero-background holders and data were taken from 10 to 80 degrees 2θ (step size of 0.4 degrees). Phase identification and quantification was carried out using JADE software in conjunction with the International Centre for Diffraction Data (ICDD) database.

2.5 Scanning electron microscopy (SEM)

After the solubility experiments and subsequent washing and drying, gibbsite samples were deposited on carbon coated aluminum stubs and then carbon coated with approximately 10 nm of carbon. SEM micrographs were then collected using a Helios Nanolab 600i SEM (FEI, Hillsoboro, OR) microscope. Micrographs were collected with an acceleration voltage of 5 kV and a current of 86 pA.

2.6 Raman Spectroscopy

Spectra were acquired using a Horiba LabRam HR spectrometer installed on a Nikon Ti-E inverted microscope using a continuous 632.81 nm laser, a 40x objective and data was acquired between 100 – 3900 cm^{-1}. A select region spanning between 450 – 790 cm^{-1} contains diagnostic Raman peaks for $Al(OH)_4^-$ ions, and this region was deconvoluted using a single polynomial to remove the background followed by regression of Lorentzian line shape parameters.

2.3 Nuclear Magnetic Resonance Spectroscopy

Liquid state ^{23}Na and ^{27}Al NMR spectra were acquired on a Varian-Inova 17.6 T NMR spectrometer utilizing a 5 mm, broad band observe (BBO), probe operating at 298 K, where the temperature was calibrated using the ^{1}H chemical shifts of ethylene glycol.[43] The corresponding ^{23}Na and ^{27}Al Larmor frequency are 198.424 and 195.460 MHz, respectively. In an N_2-filled glovebox, samples were placed in 4 mm outer diameter (o.d.) fluorinated ethylene polypropylene copolymer (FEP) inserts, sealed with a polytetrafluorethylene (PTFE) plug. The FEP NMR tube was coaxially inserted into a 5.0 mm o.d. NMR tube containing a reference NaCl solution, (0.76 M NaCl in H_2O (18 MΩ·cm), concentration determined via ICP-OES) or an $Al(H_2O)_6^{3+}$ solution (1.0 M $Al(NO_3)_3$ in H_2O (18 MΩ·cm)).

Single pulse, direct excitation, ^{23}Na NMR spectra were acquired with 8 transients, an acquisition time of 600 ms, a delay between transients of 5 s, and a $\pi/2$ liquid-state pulse (52 dB, 29 μs duration). Single pulse, direct excitation, ^{27}Al NMR spectra were acquired with 32 transients, an acquisition time of 600 ms, and a $\pi/2$ liquid-state pulse (56 dB, 19.5 μs duration). Tip angles were determined via a pulse width nutation experiment for the coaxial reference sample of 0.76 M NaCl or 1.0 M $Al(H_2O)_6^{3+}$ and measured chemical shifts are referenced to this NaCl or $Al(H_2O)_6^{3+}$ solution, where its resonance was assigned to 0 ppm. ^{23}Na

and ^{27}Al NMR spectra were processed in Mestrenova (version 14.01-23559, released 2019-06-07, Mestrelab Research S.L.) where the free induction decay was zero-filled to 1.68 s and 10 Hz line broadening was applied. The full width at half maximum line shape parameter was determined using a pure Lorentzian line shape in Mestrenova.

Pulsed field gradient NMR experiments were also conducted on the BBO probe at a field strength of 17.6 T at 298 K. ^{1}H NMR spectra were acquired using the DOSY gradient compensated stimulated echo with spin lock and convection compensation (DgcsteSL_cc) pulse sequence. The spatially dependent gradient pulse duration was 0.6 ms, and the gradient pulse strength was incremented 16 times. Pulses in DgcsteSL_cc utilized the calibrated 90° tip angle and the gradient pulse strength array was held constant for each sample within the ^{1}H PFG-NMR study. The delay between spatially dependent gradient pulses was 200 ms. The acquisition time was 2726 ms, 2 transients were detected, and the delay between experiments was 25 seconds. The reported diffusion value is the average of 2 experiments, where the second experiment utilized the DgcsteSL_cc pulse sequence with a 27 ms delay between spatially dependent gradient pulses and a 1.6 ms pulse duration, with otherwise identical settings between experiments.

Pulsed field gradient ^{23}Na NMR spectra were acquired using the bipolar gradient pulse pair stimulated echo with convection compensation (Dbppste_cc) pulse sequence. The spatially dependent gradient pulse duration was 8.6 ms, and the gradient pulse strength was incremented 16 times. Pulses in Dbppste_cc utilized the calibrated 90° tip angle and the gradient pulse strength array was held constant for each sample within the ^{23}Na PFG-NMR study. The delay between spatially dependent gradient pulses was 32 ms. The acquisition time was 800 ms, 8 transients were collected, and the delay between experiments was 2 seconds. The reported diffusion value is the average of 3 experiments with identical parameters.

Pulsed field gradient ^{27}Al NMR spectra were acquired using the Dbppste_cc pulse sequence. The spatially dependent gradient pulse duration was 10.2 ms, and the gradient pulse strength was incremented 16 times. Pulses in Dbppste_cc utilized the calibrated 90° tip angle and the gradient pulse strength array was held constant for each sample within the ^{27}Al PFG-NMR study. The delay between spatially dependent gradient pulses was 36 ms. The acquisition time was 600 ms, 64 transients were collected, and the delay

between experiments was 2 seconds. The reported diffusion value is the average of 3 experiments with identical parameters.

For the ^{1}H, ^{23}Na and ^{27}Al PFG-NMR experiments, the diffusion coefficients were calculated in vNMRJ (v 3.2) using single-component spline modeling (splmod), where the gcal parameter was calibrated with a measurement of ^{1}H diffusion of trace H_2O in D_2O at 25°C.[44] The standard deviation (± 1σ) in these measurements originates from the residual between the integrated intensity and Stejskal-Tanner relationship[45,46], and this standard deviation is propagated when averaging measurements.

3.0 Results and Discussion

This section is organized into the following logical flow. ICP-OES was first used to quantify the disparate solubilities of gibbsite in NaOH/D solutions. Gibbsite was added in excess of the solubility in solution, and the residual solid was characterized with XRD and SEM. To better understand the origin of the isotope-dependent solubilities, solution aluminum speciation was then characterized using Raman and ^{27}Al NMR spectroscopy. Under the explored solution conditions, the aluminate monomer was the only observed species and gibbsite was the only observable solid-phase. Therefore the rheological properties of the protonated and deuterated systems were quantified through analysis of diffusion coefficients with PFG-NMR spectroscopy, and a correlation between diffusivity and solubility was identified.

The equation describing gibbsite solubility in hydroxide is shown in **Eq**. **1**. Under the assumption that there is complete substitution of the H atoms by D atoms in the solvent and that minimal hydrogen exchange occurs between gibbsite and the solution phase, the equation describing gibbsite solubility in deuteroxide is

$$Al(OH)_3(s) + OD^-(aq) \rightleftharpoons Al(OH)_3OD^-(aq) \qquad (2)$$

The gibbsite solubility equation in deuterium ICP-OES results were analyzed to determine the reaction quotient (Q), which is the measurable concentration ratio of the products and reactants shown in **Eqs**. **1** and **2** at any time during the reaction:

$$Q = \frac{[\mathrm{Al(OH)_4^-}]}{[\mathrm{OH^-}]} \quad (3)$$

$$Q = \frac{[\mathrm{Al(OH)_3OD^-}]}{[\mathrm{OD^-}]} \quad (4)$$

In both cases, the aluminate ion can be measured directly by obtaining the total aluminum concentration in solution. The hydroxide/deuteroxide ion in the denominator in **Eqs**. **3** and **4** is the free hydroxide/deuteroxide concentration that is not bound to aluminum. The concentration for the free hydroxide/deuteroxide was calculated by subtracting the aluminum concentration from the total sodium concentration (satisfying the balance of charge). Therefore, the reaction quotient in terms of measurable species in solution is given by

$$Q = \frac{[\mathrm{Al}]}{[\mathrm{Na}]_\mathrm{T} - [\mathrm{Al}]} \quad (5)$$

where the subscript T denotes the total measured sodium concentration (ICP-OES). Note that neither protium nor deuterium are present in **Eq**. **5**. Therefore, under the assumptions described above, the reaction quotient can be defined using **Eq**. **5** for any combination of protium and deuterium (e.g. a 1:1 mixture as used in this experiment).

At equilibrium the measured reaction quotient is the apparent solubility constant (K').

$$Q_{Eq} = K' \quad (6)$$

3.1 ICP-OES measurements indicated enhanced gibbsite solubilities in deuterated systems

The reaction quotient over time for the 2.4 mol·kg^{-1} (**A**) and the 3.3 mol·kg^{-1} (**B**) experiment at ratios of 1:0, 1:1, and 0:1 protium to deuterium is shown in **Figure 1**. Aluminate concentration (i.e. gibbsite dissolution) is proportional to the reaction quotient. For every case, the initial rates of gibbsite dissolution were indistinguishable from one another. The concentration of aluminum was noticeably different for each mixture at about 3 h for the 2.4 mol·kg^{-1} experiment and 4 h for the 3.3 mol·kg^{-1} experiment, with the concentration increasing as a function of the total amount of deuterium in solution. Equilibrium conditions, defined as a constant aluminum concentration in solution, were established after ~11 h.

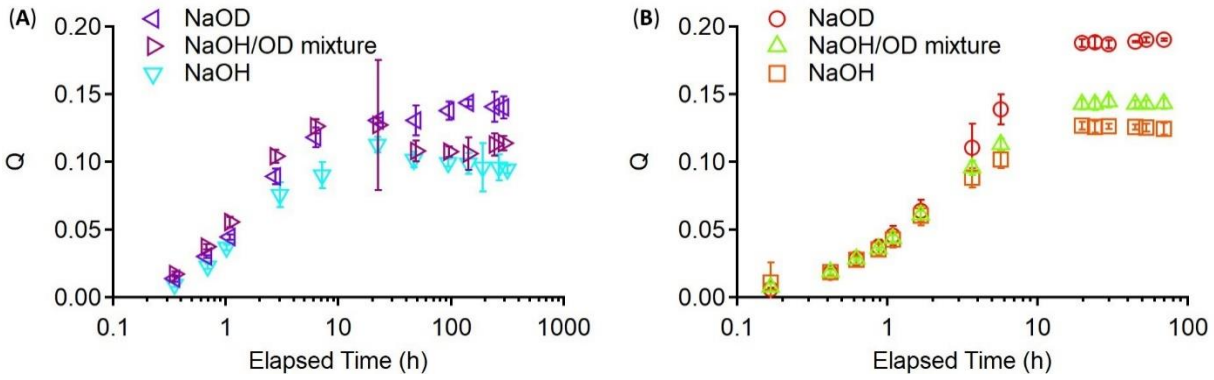

Figure 1. The reaction quotient for gibbsite dissolution in 2.4 mol·kg^{-1} NaOH/OD (**A**) and 3.3 mol·kg^{-1} NaOH/OD (**B**) was monitored over time using ICP-OES. Each point represents the average (± 3 σ) of three separate experiments. Equilibrium was assumed to be reached when no more changes were observed in the reaction quotients.

At equilibrium the measured reaction quotient is the apparent solubility constant for gibbsite (K'). The K' values (the average of 6 time points) for each experiment are shown in **Figure 2**. Note that **Figure 2** shows the rate constants as a function of the solution composition in terms of deuterium (x_D), where x_D = moles of deuterium / (moles of deuterium / moles of protium). The value of $x_{D\ comp}$ conveniently quantifies the relative amount of deuterium in solution and is used in the remainder of this manuscript. A significant increase in the K' with increasing amounts of deuterium relative to protium was found in both the 2.4 and 3.3 mol·kg^{-1} experiment. The $K'$of aluminum at equilibrium was found to be 0.098 ± 0.003 in 2.4 mol·kg^{-1} NaOH, which agreed well with the solubility measurements of gibbsite at similar compositions obtained by Wesolowski, et al.[47] The K' increased to 0.113 ± 0.008 and 0.137 ± 0.005 in the 1:1 and 0:1 H:D ratios,

respectively. This corresponded to nearly a 40% increase in the apparent solubility, when substituting protium with deuterium.

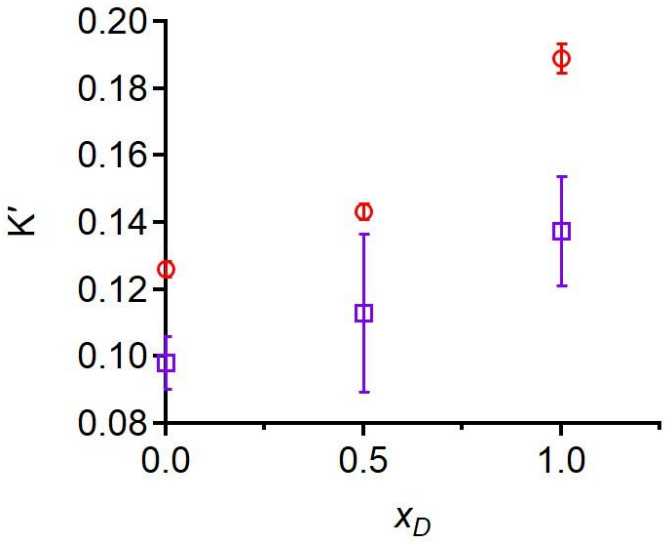

Figure 2. The apparent equilibrium constants for gibbsite solubility in 2.4 mol·kg^{-1} (purple squares) and 3.3 mol·kg^{-1} (red circles) NaOH/D are shown for different amounts of deuterium. Each point on the plot represents the average (± 3 σ) of 6 time points when equilibrium was reached.

Similar results were observed for the 3.3 mol·kg^{-1} experiments also shown in **Figure 2**. The K' was 0.126 ± 0.001 in the 3.3 mol·kg^{-1} NaOH case and then increased to 0.143 ± 0.001 and 0.189 ± 0.001 for the 1:1 and 0:1 H:D ratios, respectively. This corresponded to a 50% increase in solubility when protium is substituted by deuterium. These data show that the increase in solubility in deuterated conditions becomes more pronounced as the concentration of total sodium becomes larger. One explanation could be due to the increased divergence from ideal conditions caused by an increase in sodium and deuteroxide ions in solution, which would make specific ion effects (or isotopic effects) more pronounced. However the gibbsite solubility over a larger total concentration range would need to be investigated, as isotopic effects are often nonlinear.[36] As can be seen in **Figure 2**, the increase in K' is proportional to an increase in deuteration in both the 2.4 (purples squares) and 3.3 (red circles) mol·kg^{-1} cases.

3.2 XRD and scanning electron microscopy confirm that gibbsite is the solid in equilibrium with solution in all systems

Loh et al. hypothesized that the more soluble gibbsite polymorph bayerite was preferentially formed in deuteroxide and that this explained the difference in their solubility results.[39] Loh et al. also noted differences in gibbsite solubility and precipitation products from supersaturated solutions seeded with gibbsite at elevated temperatures.[39] The physical explanation for the increase in solubility is difficult to determine by solubility studies alone, as no information is obtained on speciation, solvation, or translational dynamics.

In these experiments, pXRD analysis (**Figure 3** and **Figures S.1** – **S.3**) showed no evidence for the formation of bayerite, or any other Al-bearing phase, such as sodium aluminate hydrates. **Figure S.2** contains an example pXRD diffraction pattern for gibbsite, and for a mixture of gibbsite and bayerite, highlighting the sensitivity of the diffractogram to the presence of bayerite which is detected by the (001) peak among others. A key observation which possibly explains the formation of bayerite in the study by Loh et al. was that, prior to pXRD analysis, bayerite was formed when drying solids in an oven with trace amounts of residual sodium hydroxide/deuteroxide solution present (**Figure S.3, 4** and **5)**. This may be due to the dramatic increase in local concentrations of Na^+ and OH/OD^- ions during the drying process, which would change the favored precipitation product. In this case, the kinetically favored precipitation product may be bayerite, even though it is less stable.[25] The pXRD results for gibbsite are complex, with small but definite shifts in the gibbsite peak positions in the diffractograms when deuterium is present compared to the pure protium experiment, and in the presence of residual Na^+ during drying (**Figure 3**). However, it is clear that gibbsite is the dominant phase when the solids are washed thoroughly with water prior to drying and pXRD analysis, and so it is likely that the present of bayerite in the study by Loh et al. was due to transformation of the precipitated solids from gibbsite to bayerite due to incomplete removal of caustic solution.

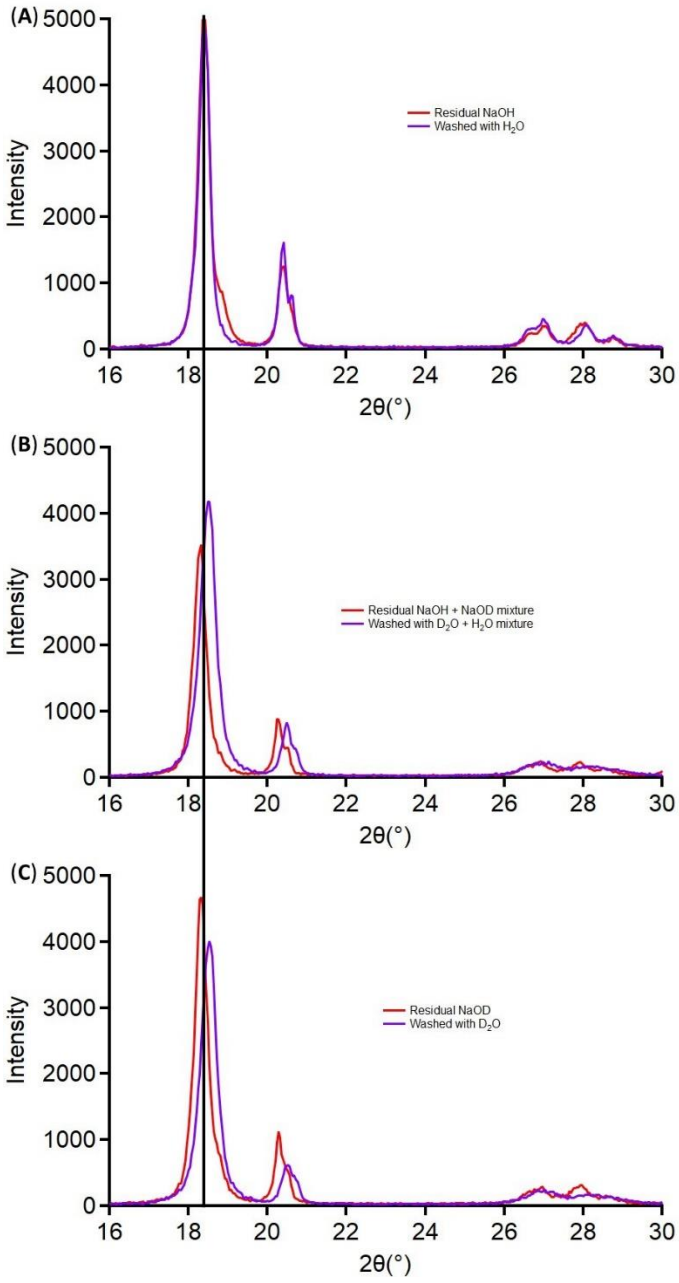

311

312 **Figure 3**. Powder X-ray diffraction results showing the
313 effect of not washing the solids prior to XRD analysis for
314 the 1:0 (**A**), 1:1 (**B**), and 0:1 **(C**) H:D ratio 3.3 mol·kg^{-1}
315 NaOH/D experiments. The solid line indicates the position
316 of the center of the gibbsite diffraction peak for the pure
317 protium experiment. No bayerite was found in these
318 samples

319 Additionally, SEM images of gibbsite after reaction with 3.3 mol·kg^{-1} NaOH/D showed that particle

320 morphology remained as nanoplates, with lengths < 600 nm, and an approximate length to thickness ratio

of 10:1 (**Figures 4** and **5**). The lack of significant changes in size and shape of the gibbsite particles relative to the as-synthesized gibbsite indicates that alternative phenomena are needed to explain the differences in gibbsite solubility for the 1:0, 1:1, and 0:1 H:D solubility experiments.

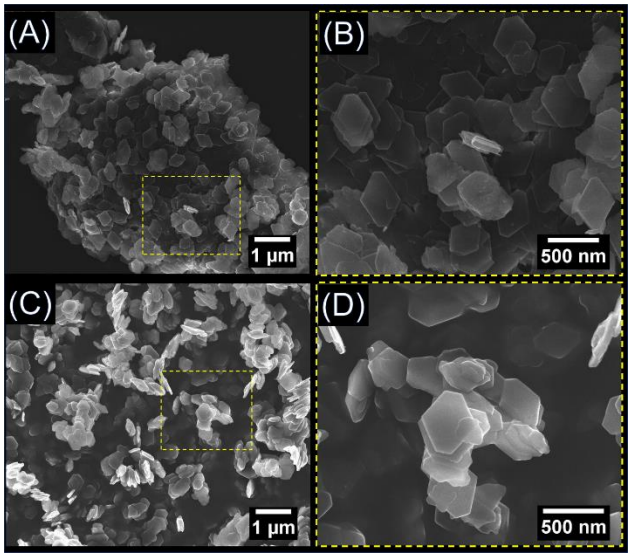

Figure 4. Scanning electron micrographs of (A) the precursor gibbsite and (B) the precursor gibbsite at a higher magnification. Additional micrographs of (C) gibbsite reacted in 3.3 mol·kg^{-1} NaOH and (D) gibbsite reacted in 3.3 mol·kg^{-1} NaOH at a higher magnification. The yellow dashed square indicates the approximate area selected for the higher magnification micrograph.

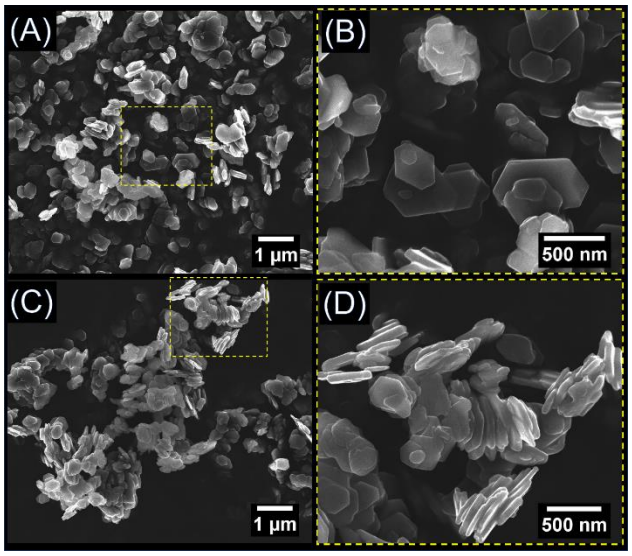

Figure 5 Scanning electron micrographs of (A) gibbsite reacted in 3.3 mol·kg^{-1} NaOH/D and (B) gibbsite reacted in 3.3 mol·kg^{-1} NaOH/D at a higher magnification. Additional micrographs of (C) gibbsite reacted in 3.3 mol·kg^{-1} NaOD and (D) gibbsite reacted in 3.4 m at NaOD at a higher magnification. The yellow dashed square indicates the approximate area selected for the higher magnification micrograph.

335 *3.3 Liquid state NMR and Raman spectroscopy indicate solution speciation is independent of*
336 *isotopic substitution*

337 In order to gain insight into the causes of the increase in gibbsite solubility in deuterated solutions,
338 and complement the ICP-OES study, ^{27}Al and ^{23}Na NMR spectroscopy was performed on the equilibrated
339 solutions described above (the last 6 time points from each of the experiments in **Figure 1**). One ^{27}Al
340 resonance was found in the NMR spectra for each condition, indicating that the exchange between protiated
341 and deuterated hydroxides ligating the aluminate ion are fast relative to the NMR timescale, and therefore
342 a single resonance is observed which is the average of Al ligated by protiated or deuterated hydroxides in
343 mixed systems. The ^{27}Al resonance was referenced to a physically separated coaxial insert containing
344 $Al(H_2O)_6^{3+}$, which appears at 0 ppm (**Figures S.4** and **S.5**). Analysis of the chemical shift and normalized
345 intensity for the ^{27}Al NMR resonance corresponding to tetrahedrally coordinated aluminate (≈ 80
346 ppm)[28,48,49] is shown in **Figure 6**. For each panel in **Figure 6**, the purple squares (2.4 mol·kg^{-1}) and red
347 circles (3.3 mol·kg^{-1}) represent the average (± 3 σ) of the 3 separate solubility experiments. ^{23}Na NMR
348 spectroscopy was performed on the 3.3 mol·kg^{-1} experiment and the peak analysis is shown in **Figure S.6**.

349 In addition, NMR spectroscopy was used to verify the increased gibbsite solubility found in
350 deuterated solutions using ICP-OES. An increase in the total integrated intensity of the ^{27}Al resonance was
351 observed in the both the 2.4 and 3.3 mol·kg^{-1} NaOH/D experiments (**Figure 6(C)**). The K' (**Figure 6(D)**)
352 was determined from the NMR data (**Eqs. 5** and **6**) for the 3.3 mol·kg^{-1} NaOH/D experiment, using the total
353 integrated intensity of the ^{27}Al and ^{23}Na peak to represent the total aluminate concentration and total sodium
354 concentration, respectively (**Figure 6(C)** and **Figure S.6(C)**). While the K' was slightly larger (albeit within
355 2σ of each other) for the NMR results compared to the ICP-OES results, a clear increasing trend with total
356 deuterium was established. The reason for the slight discrepancy between the NMR and ICP-OES results
357 may be due to the relative uncertainty in the ^{23}Na and ^{27}Al integrated intensity measurements leading to a
358 greater standard deviation for *K*' for measurements performed in triplicate compared to ICP-OES.
359

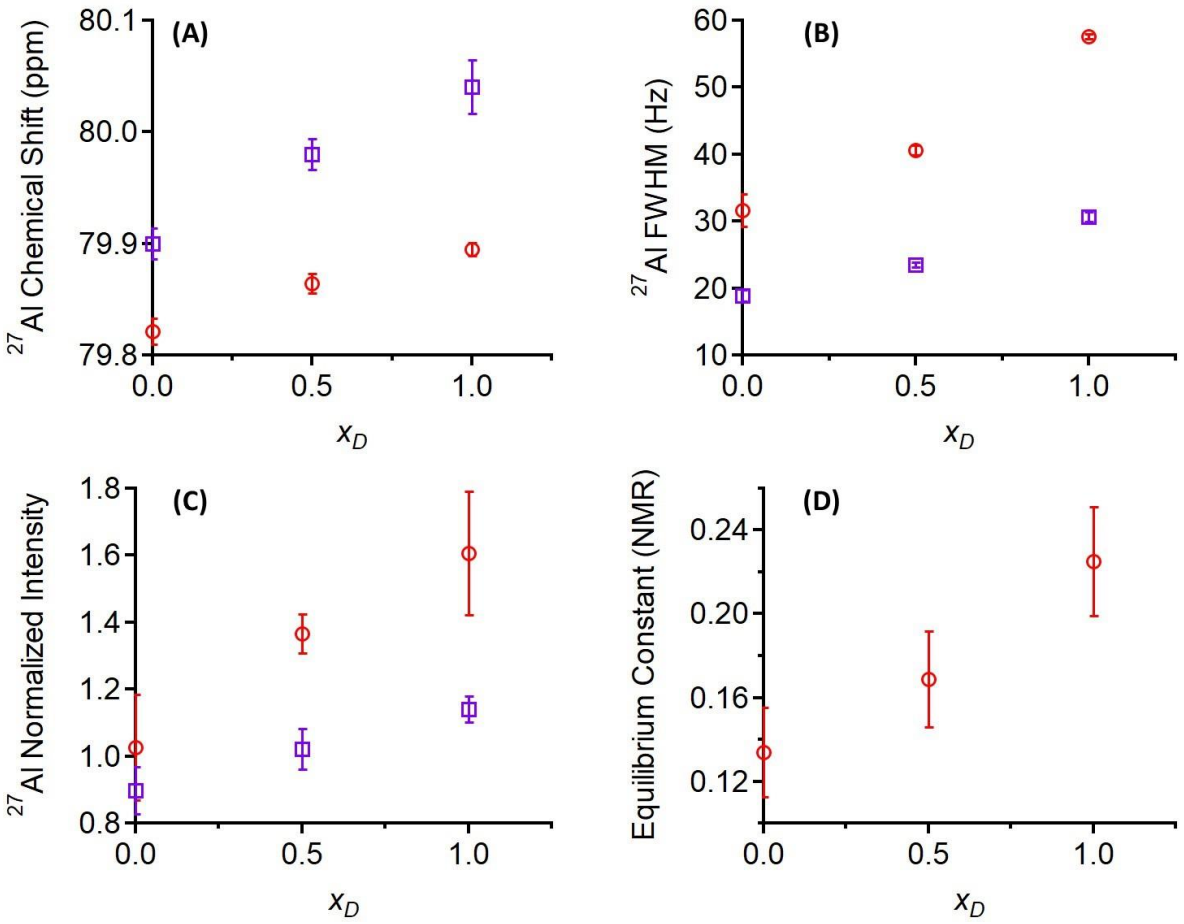

Figure 6. The tetrahedral ^{27}Al NMR resonance of the aluminate ion at equilibrium is compared at different ratios of deuterium for the 2.4 mol·kg^{-1} NaOH/D experiment (purple squares) and 3.3 mol·kg^{-1} NaOH/D experiment (red circles). The ^{27}Al chemical shift (**A**), FWHM (**B**), integrated intensity (**C**), and the NMR determined equilibrium constant (**D**) are shown. Each point represents the average (± 3 σ) results of 3 separate experiments in panels **A** – **C**. The equilibrium values and uncertainty (± 1 σ) shown in panel **D** were calculated using the average normalized ^{27}Al integrated intensity and average normalized ^{23}Na integrated intensity as described in the text.

The aluminate ^{27}Al chemical shift was found to be 79.90 ± 0.01 ppm in the 2.4 mol·kg^{-1} and 79.82 ± 0.01 ppm in the 3.3 mol·kg^{-1} experiment (1:0 H:D ratio), which agreed well with previously reported data.[48] While the chemical shift increased to higher frequencies for deuterated samples both the 2.4 and 3.3 mol·kg^{-1} experiments (**Figure 6**(**A**)), the change was small (< 0.1 ppm). An increase in the observed chemical shift corresponds to a deshielding of the aluminum atom in the aluminate ion. This may indicate that the electron density is more delocalized around the aluminate ion in the 0:1 H:D experiment, which may reflect changes in the aluminate ligand chemistry that results in increased stability in the solubility experiments of the deuterated systems.

The full-width at half max (FWHM) of the ^{27}Al NMR aluminate peak was larger in 3.3 mol·kg^{-1} experiments compared to the 2.4 mol·kg^{-1} experiments and increased with the amount of deuteration (**Figure 6**(**B**)). The FWHM was 18.9 ± 0.8, 23.4 ± 0.4, 30.7 ± 0.8 Hz (average ± 3 σ, in order of increasing H:D ratio) and 31.6 ± 2.5, 40.5 ± 0.7, 57.6 ± 0.4 Hz (average ± 3 σ, in order of increasing H:D ratio) for the 2.4 and 3.3 mol·kg^{-1} experiments, respectively. There are many factors that contribute to the breath of the NMR resonance, including chemical exchange between multiple species, viscosity, and magnetic field inhomongeneity.[50] The broadening is not likely due to the existence of multiple aluminum species because only $Al(OH)_4^-$ is detected under these conditions with Raman spectroscopy (**Figure 7**).[25,47,48,51]

Since the chemical shift change is small with increasing deuteroxide (**Figure 6**(**A**)), it could be argued that broadening of the peak in the deuterated solutions is caused by varying degrees of deuterium substitution on the aluminate ion. However, this is also unlikely because an increase in the FWHM is observed going from the 1:1 to the 0:1 H:D ratio experiments, where it is expected that the variance in the degree of deuterium substitution would be highest in the 1:1 H:D ratio experiment. This is because the binding constants for different possible combinations of deuterium substitution are dependent on the ligand (hydroxide or deuteroxide ion) concentration and there would be the largest amount of ligand competition when the concentrations are equal. Therefore, it is likely that the aluminate peak broadening in the deuterated solutions is caused by differences in diffusive motion through an increase in viscosity. The ^{23}Na NMR resonances' FWHM (**Figure S.6**(**B**)) followed the trend of the ^{27}Al NMR resonances' FWHM, increasing with an increase in the total amount of deuterium. This is consistent with the FWHM being dependent on the viscosity of solutions since the spectroscopic properties of the aluminate anions and sodium cations are similar in deuterated solvents.

The ^{27}Al chemical shift may be attributed, in part, to the difference in the hydrogen bonding energies associated with deuterated and non-deuterated aqueous solutions which originates from differences in the zero-point vibrational energies of deuterated and non-deuterated molecules.[32] The net effect of isotopic substitution on the vibrational modes of the solution species can be measured using Raman Spectroscopy (**Figure 7**), however connecting that information to the energy of a molecule, an ion, and the

hydrogen bonding network is complex.[33,52] The Raman results confirm the presence of a single aluminum species, aluminate (**Figure 7**(**A**)). In addition the expected appearance of vibrational modes caused by the substitution of H with the heavier D atoms for both the hydroxide and water regions were present (**Figure 7**(**B**)).[33,53] The presence of aluminate monomers as the predominant species at these concentrations agrees with the Raman results of Graham et al. (2018), who evaluated solutions prepared at 3 M NaOH with various amounts of dissolved Al produced via dissolution of gibbsite and found that the Raman region of the Al-O bands contained only a single band attributed to aluminate monomers in solution.[31]

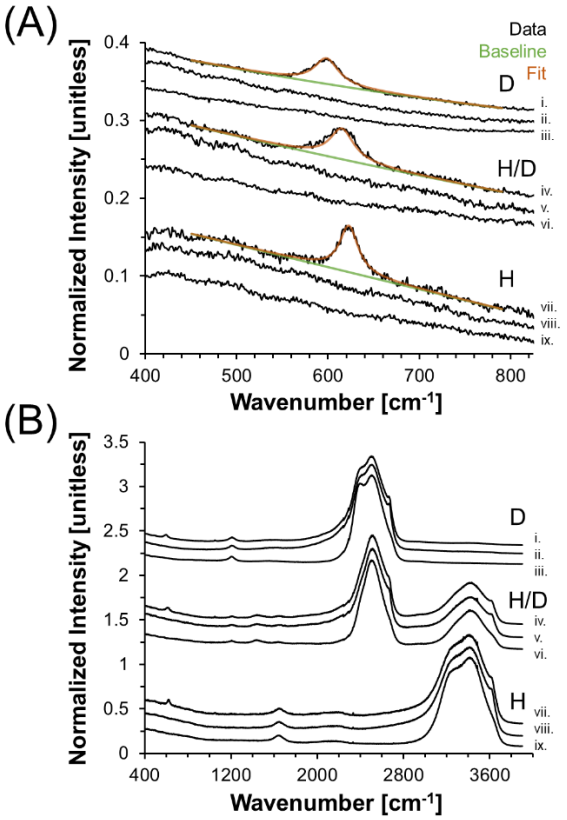

Figure 7. Raman spectra showing (**A**) Al-O region and (**B**) the full spectral window. The spectra are normalized to the maximum intensity of the OX stretching region. Spectra are vertically offset from one another. The solutions for both spectra are labeled: (i). 3.3 mol·kg^{-1} NaOD experiment after addition of gibbsite (ii.) 3.3 mol·kg^{-1} NaOD experiment before addition of gibbsite (iii). D_2O solution (iv). 3.3 mol·kg^{-1} NaOH/D experiment after addition of gibbsite (v.) 3.3 mol·kg^{-1} NaOH/D experiment before addition of

gibbsite (vi). $(H/D)_2O$ solution (vii). 3.3 $mol \cdot kg^{-1}$ NaOH experiment after addition of gibbsite (viii.) 3.3 $mol \cdot kg^{-1}$ NaOH experiment before addition of gibbsite (ix.) H_2O solution

Raman spectra were acquired on H:D solutions to inspect isotope effects on the OX stretching region, X_2O bending region, and the $Al(OH)_4^-$ vibrational motion. **Table 2**. shows the parameter results after deconvolution. The Raman spectra are shown in **Figure 7**. For each ratio of H:D, spectra were acquired of the Al-containing solution, the Al-free background electrolyte NaOH/D solution, and an electrolyte-free aqueous solution. Inspection of the Al-O region in **Figure 7**(**A**) indicates $Al(OX)_4^-$ is the primary form of Al in solution because bands primarily associated with $Al_2O(OH)_6^{2-}$ at 535 and 700 cm^{-1} are absent.[28,54] There is demonstrably a greater FWHM of the Raman band of $Al(OX)_4^-$ in deuterated system and deuterium substitution results in the band appearing at lower wavenumber. Both the greater FWHM (31.9 versus 24.7 cm^{-1}) and the shift to lower wavenumbers by ca. 20 cm^{-1} are consistent with prior literature that compared the infra-red and Raman spectroscopies of protoniated and deuterated sodium aluminate solutions.[54]

Table 2. Deconvolution parameters for the Al-O Raman band.

	Peak Position [cm^{-1}]	**FWHM [cm^{-1}]**
D	598.2	31.9
H/D	615.1	31.3
H	622.7	24.7

In addition to providing information on aluminate ion speciation, the OH stretching and OD stretching regions are resolved from one another as shown in **Figure 7**(**B**). Dissolution of NaOH/D manifests in a sharp band forming at high wavenumber in either the OD or OH stretching region at 2500 and 3200 cm^{-1} respectively, in addition to a broad band at lower wavenumbers of 2300 and 3000 cm^{-1}. The OD and OH stretching region for mixtures of H:D is demonstrably unique from the isotopically pure solutions. In the absence of dissolved salt, the broad peaks at lower wavenumbers of 2300 and 3000 cm^{-1} are absent from the spectra. This feature is typically assigned to a large network of water and its absence in mixtures is interpreted as being indicative of a disruption in the extended hydrogen bond network due to deuterium substitution. The H_2O bending region (1200 – 1600 cm^{-1}) is also sensitive to deuterium

substitution, and in mixtures of H and D a third band appears in this region in addition to the bands at 1200 cm^{-1} and 1600 cm^{-1} in isotopically pure solutions.

3.4 Liquid state pulsed field gradient NMR diffusometry reveals elevated viscosities in deuterated systems

To further investigate the underlying causes of increased gibbsite solubility in NaOD compared to NaOH, ^{1}H, ^{23}Na, and ^{27}Al PFG-NMR spectroscopy was used to probe the solution rheology and transport properties of the system. PFG-NMR employs spatially-dependent magnetic field gradients to determine the diffusion coefficients (D_{diff}) of resonances through the Stejskal-Tanner relationship.[45,46] ^{1}H, ^{23}Na, and ^{27}Al diffusion coefficients were determined in a 1:0, 1:1, and 0:1 H:D ratio 2.4 m NaOX in X_2O solution (where X is H, D, or a mixture of the two). For each nucleus, a decrease in the diffusion coefficient was found as the amount of deuterium increased (**Figure 8**). The ^{1}H D_{diff} (red circles in **Figure 8**) decreased from $(15.7 \pm 0.2)\times10^{-10}$ m^2s^{-1} in the pure protium experiment to (14.0 ± 0.1) and $(12.0 \pm 0.3)\times10^{-10}$ m^2s^{-1} in the 1:1 and 0:1 H:D experiments, respectively. The ^{23}Na D_{diff} (purple triangles in **Figure 8**) were found to be (11.9 ± 0.1), (9.9 ± 0.1), and $(8.9 \pm 0.1)\times10^{-10}$ m^2s^{-1} and the ^{27}Al D_{diff} (green squares in **Figure 8**) were (7.3 ± 0.1), (6.5 ± 0.2), and $(5.5 \pm 0.2)\times10^{-10}$ m^2s^{-1} in the 1:0, 1:1, and 0:1 H:D ratio, respectively. Additional ^{1}H PFG-NMR spectroscopy was performed on solutions of 4 and 6 $mol\cdot kg^{-1}$ total sodium at various deuterium ratios. The resulting diffusion coefficients are shown in **Figure S.7**. For every concentration used, the D_{diff} decreased at a similar rate from the diffusion coefficient of the pure protium case ($D_{diff,H}$) as the concentration of deuterium increased. Therefore, in order to get an estimate of how the diffusion coefficients change as a function of total Na concentration, the ratio of the diffusion coefficient measured for ^{1}H (D_{diff}^{1H}) and the ^{1}H diffusion coefficient measured in the pure protium case ($D_{diff,H}^{1H}$) was calculated for the 2 and 4 $mol\cdot kg^{-1}$ PFG-NMR experiments. The results of this ratio are shown in **Table 3**.

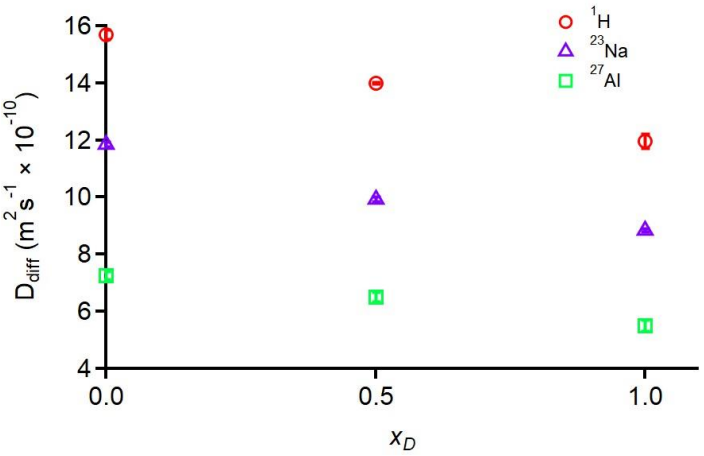

Figure 8. The diffusion coefficients for ^{1}H (red circles), ^{23}Na (purple triangles), ^{27}Al (green squares) in 2 mol·kg^{-1} total sodium solutions are shown as a function of the total ratio of deuterium. A deuterium ratio of 1.0 corresponds to the 0:1 H:D. The error bars are smaller than the marker for most of the points.

Oligomeric intermediates have previously been shown to be important in the precipitation reaction of aluminum hydroxides.[55–57] It should be noted that the gibbsite solubility equilibrium shown in **Eq**. **1** includes the precipitation reaction, which is the reverse of the dissolution reaction. The equilibrium constant can be written as the ratio of the dissolution (k_{diss}) and precipitation (k_{ppt}) reaction rate constants. At equilibrium, the relationship shown in **Eq**. **7** holds.

$$k_{diss}[OH^-] = k_{ppt}[Al(OH)_4^-] \quad (7)$$

Since there was little difference in the dissolution reaction rates (**Figure 1**) when deuterated solutions were used, it seems likely that the ratio of the dissolution reaction rate can be considered close to 1 between the 1:0, 1:1, and 0:1 ratios of H:D. A similar relationship has been shown for lithium (Li) isotope fractionation during uptake by gibbsite, where Li isotopes are not significantly fractionated during mineral dissolution, but are highly sensitive to formation of precipitates that preferentially uptake the lighter isotope, leaving the heavier isotope enriched in solution.[58] Therefore, the increased solubility in deuterated solutions is the result of a slower precipitation rate from deuterated sodium hydroxide solutions. This is true even

with an increase in the reactant concentration for the precipitation reaction (the concentration of aluminate). Therefore, there must be some factor in the precipitation rate constants that impedes precipitation. Assuming that oligomeric intermediates involving ligand dissociation and/or condensation of $Al(OH)_4^-$ are important for precipitation and nucleation to occur, a simple model to describe the reaction involves two $Al(OH)_4^-$ monomers diffusing together to form a aggregated intermediate. The intermediate can either precipitate into a solid phase or break apart into two $Al(OH)_4^-$ monomers. In a diffusion dominated reaction it can be shown[59] that, under the steady-state approximation (the transition state aggregated cluster rate of change is 0), the precipitation reaction rate (see derivation in the **SI**) can be given by:

$$Rate \propto k_{diff}[Al]_{Eq}{}^2 \quad \textbf{(8)}$$

where k_{diff} is the diffusion-controlled rate constant and $[Al]_{Eq}$ is the concentration of aluminum at equilibrium. The k_{diff} (**S.7**) is proportional to the diffusion coefficients of the reactants. In this case, since we have ^{1}H diffusion coefficients $\left(D_{diff}^{1H}\right)$ in multiple total Na concentrations, and since the ^{23}Na and ^{27}Al diffusional coefficients change similarly to the ^{1}H coefficients with the amount of deuterium added, the D_{diff}^{1H} values are used as an estimate of the total diffusional coefficients for the reactants in 2.4 and 3.3 mol·kg^{-1} experiments. To compare the relative rates of the reaction between the different amounts of deuterium, the ratio of the ^{1}H diffusion coefficient measured (D_{diff}^{1H}) and the $D_{diff,H}^{1H}$ was used as an estimate of the relative difference in total diffusivity for the different solubility reactions (**Table 3**). This allows for the inverse ratio (since the reverse of the dissolution reaction is of interest) of the measured apparent solubility constant in any experimental condition K' and the measured apparent solubility constant in the 1:0 H:D experiment (K_H') to be compared directly to the relative change in diffusion coefficients (**Table 3**).

Table 3. The relative change in ^{1}H diffusion coefficients are compared to the difference in apparent solubility constants.

Experiment	$\frac{D_{diff}^{1H}}{D_{diff,H}^{1H}}$	$\left(\frac{K'}{K'_H}\right)^{-1}$
2.4 mol·kg^{-1} 1:0 H:D	1.00	1.00
2.4 mol·kg^{-1} 1:1 H:D	0.89	0.87
2.4 mol·kg^{-1} 0:1 H:D	0.76	0.71
3.3 mol·kg^{-1} 1:0 H:D	1.00	1.00
3.3 mol·kg^{-1} 1:1 H:D	0.84	0.88
3.3 mol·kg^{-1} 0:1 H:D	0.72	0.67

The values in **Table 3** show that the change in relative diffusion of ^{1}H is similar to the relative difference in gibbsite solubility observed in the 1:0, 1:1, and 0:1 H:D experiments. This implies that the simple diffusion limited model, requiring $Al(OH)_4^-$ clusters to come together before precipitation can occur, may explain the solubility results. Given that a decrease in electron density around the ions (deshielding) in the ^{23}Na and ^{27}Al NMR data was observed when the ratio of deuterium was increased for both the 2.4 and 3.3 mol·kg^{-1} experiments, it is possible that the cause of the decrease in rate of diffusion is due to a strengthening of the hydrogen bonding network in the deuterated experimental conditions It should be noted that in a classical reaction mechanism, the forward and reverse reactions should be affected in the same way: the strengthening of the hydrogen bond network should impede the precipitation and dissolution reaction rates. However, it has been demonstrated that surface effects (such as the amount of the different types of Al coordination species and the surficial interaction of Na) play a significant role in the reactions of gibbsite synthesized at circumneutral conditions.[30] Here, we propose that the rate of the precipitation is controlled by the diffusion of oligomers and the ability to form intermediate species, whereas dissolution is a interfacial reaction controlled by the amount of coordinated Al species and Na at the gibbsite surface. The dissolution reaction would therefore not be as affected by the strength of the hydrogen bond network. The observation that we did not see a significant difference in the rate of dissolution between the different experiments supports this assumption.

As the deuterated/protonated aluminate ion in **Eq. 2** reprecipitates and redissolves with protiated gibbsite in the deuterated solution, it is likely that the remaining hydrogen atoms in the protiated gibbsite

are substituted by deuterium, therefore introducing H atoms in the solution. However, gibbsite solubility is small compared to the total concentration of deuterium in solution,[47] even in 3.3 mol·kg^{-1} NaOH/D (353 ± 13 mmol·kg^{-1}) and the protium/deuterium exchange will not greatly dilute the total amount of deuterium in solution. Therefore, for simple comparison purposes, this study assumes that solution composition is constant in terms of deuterium to protium ratio (either 1:0, 1:1, or 0:1 H:D). In future work, surface-sensitive spectroscopies will be used to understand how deuterium substitution influences exchange reactions at the solution-aluminum hydroxide interface, and how these exchange reactions affect the thermodynamic properties of the system.

Conclusion

The solubility of gibbsite, a major polymorph of aluminum hydroxide ($Al(OH)_3$), in NaOH and NaOD at two different total sodium concentrations (2.4 and 3.3 mol·kg^{-1}) was measured using ICP-OES and ^{27}Al NMR. Gibbsite solubility was higher in 3.3 mol·kg^{-1}, as expected based on the literature.[60] Importantly, the solubility increased as the total ratio of deuterium was increased in the solution. Comparison of diffusion coefficients measured using ^{1}H, ^{23}Na, and ^{27}Al pulsed-field gradient NMR spectroscopy showed that diffusion decreased with increasing total deuterium in solution, consistent with the notion of increasing strength in the hydrogen/deuterium bonding network. Because the formation of oligomeric intermediates should depend not only on the intermolecular collisions facilitated by both convective mixing and diffusion, but also the structural rearrangement of the hydroxide (deuteroxide) ligands, deuterium substitution alters the solubility of the system while nominally conserving the observable speciation of both the solution phase aluminate and solid phase gibbsite.

Our study also demonstrates that the strength of the hydrogen bonding network determines the diffusivity and interaction of ions and solvent molecules in solution, which is important for dissolution and precipitation pathways where oligomeric intermediates are thought to be important. We show that the ^{1}H diffusion coefficients correlate well with the measured solubility constants. This suggests that gibbsite

solubility models should consider diffusion or viscosity measurements as a potential means for predicting the net effect of complex solution compositions composed of multiple electrolytes. In other words, complex specific ion effects that influence the hydrogen bonding network may be tabulated and ranked by evaluating changes in diffusion coefficients. This could be useful for any system where the formation of oligomeric intermediates is expected to be important in the precipitation and dissolution reaction mechanism.

Acknowledgements

This research was supported by the Interfacial Dynamics in Radioactive Environments and Materials (IDREAM), an Energy Frontier Research Center funded by the U.S. Department of Energy, Office of Science, Basic Energy Sciences. NMR and Raman spectroscopy were performed using facilities at the Environmental Molecular Science Laboratory (EMSL, grid.436923.9), a DOE Office of Science User Facility sponsored by the Office of Biological and Environmental Research at Pacific Northwest National Laboratory (PNNL). PNNL is a multi-program national laboratory operated for DOE by Battelle Memorial Institute operating under Contract No. DE AC05-76RL0-1830. This research used resources of the Advanced Photon Source, a U.S. Department of Energy (DOE) Office of Science User Facility operated for the DOE Office of Science by Argonne National Laboratory under Contract No. DE-AC02-06CH11357. A.J.K. is grateful for the support from the PNNL-WSU Distinguished Graduate Research Program and the DOE-Science Graduate Student Research program.

Supporting Information

The following information can be found in the supporting information document**:** pXRD scans of materials used in this study, comparison of bayerite and gibbsite pXRD patterns, analysis of the amount of bayerite compared to gibbsite as a function of the residual NaOH, representative ^{27}Al NMR spectra of the solution phase at equilibrium, the reproducibility of the aluminate NMR shift is shown across the varying amounts of deuterium, the ^{23}Na NMR chemical shift, FWHM, and normalized intensity are shown for each

concentration of deuterium, the results of the ^{1}H diffusion coefficients shown as a function of relative amount of deuterium, and the derivation of the diffusion dominated rate constant.

References

(1) Zhang, H.; De Yoreo, J. J.; Banfield, J. F. A Unified Description of Attachment-Based Crystal Growth. *ACS Nano* **2014**, *8* (7), 6526–6530. https://doi.org/10.1021/nn503145w.

(2) Niederberger, M.; Cölfen, H. Oriented Attachment and Mesocrystals: Non-Classical Crystallization Mechanisms Based on Nanoparticle Assembly. *Phys. Chem. Chem. Phys.* **2006**, *8* (28), 3271–3287. https://doi.org/10.1039/b604589h.

(3) De Yoreo, J. J.; Gilbert, P. U. P. A.; Sommerdijk, N. A. J. M.; Penn, R. L.; Whitelam, S.; Joester, D.; Zhang, H.; Rimer, J. D.; Navrotsky, A.; Banfield, J. F.; Wallace, A. F.; Michel, F. M.; Meldrum, F. C.; Colfen, H.; Dove, P. M. Crystallization by Particle Attachment in Synthetic, Biogenic, and Geologic Environments. *Science (80-.).* **2015**, *349* (6247), aaa6760-1-aaa6760-9. https://doi.org/10.1126/science.aaa6760.

(4) Jehannin, M.; Rao, A.; Cölfen, H. New Horizons of Nonclassical Crystallization. *J. Am. Chem. Soc.* **2019**, *141* (26), 10120–10136. https://doi.org/10.1021/jacs.9b01883.

(5) Gebauer, D.; Wolf, S. E. Designing Solid Materials from Their Solute State: A Shift in Paradigms toward a Holistic Approach in Functional Materials Chemistry. *J. Am. Chem. Soc.* **2019**, *141* (11), 4490–4504. https://doi.org/10.1021/jacs.8b13231.

(6) Demichelis, R.; Raiteri, P.; Gale, J. D.; Quigley, D.; Gebauer, D. Stable Prenucleation Mineral Clusters Are Liquid-like Ionic Polymers. *Nat. Commun.* **2011**, *2*, 590. https://doi.org/10.1038/ncomms1604.

(7) Suo, L.; Borodin, O.; Gao, T.; Olguin, M.; Ho, J.; Fan, X.; Luo, C.; Wang, C.; Xu, K. "Water-in-Salt" Electrolyte Enables High-Voltage Aqueous Lithium-Ion Chemistries. *Science (80-.).* **2015**, *350* (6263), 938–943. https://doi.org/10.1126/science.aab1595.

(8) Gebauer, D.; Kellermeier, M.; Gale, J. D.; Bergström, L.; Cölfen, H. Pre-Nucleation Clusters as

Solute Precursors in Crystallisation. *Chem. Soc. Rev.* **2014**, *43* (7), 2348. https://doi.org/10.1039/c3cs60451a.

(9) Bøjesen, E. D.; Iversen, B. B. The Chemistry of Nucleation. *CrystEngComm* **2016**, *18* (43), 8332–8353. https://doi.org/10.1039/c6ce01489e.

(10) Reichenbach, J.; Wynne, K. Frustration vs Prenucleation: Understanding the Surprising Stability of Supersaturated Sodium Thiosulfate Solutions. *J. Phys. Chem. B* **2018**, *122* (30), 7590–7596. https://doi.org/10.1021/acs.jpcb.8b04112.

(11) Bird, M. I.; Longstaffe, F. J.; Fyfe, W. S.; Tazaki, K.; Chivas, A. R. Oxygen-Isotope Fractionation in Gibbsite: Synthesis Experiments versus Natural Samples. *Geochim. Cosmochim. Acta* **1994**, *58* (23), 5267–5277. https://doi.org/10.1016/0016-7037(94)90310-7.

(12) Fernandes, K.; Marques Júnior, J.; Bahia, A. S. R. de S.; Demattê, J. A. M.; Ribon, A. A. Landscape-Scale Spatial Variability of Kaolinite-Gibbsite Ratio in Tropical Soils Detected by Diffuse Reflectance Spectroscopy. *Catena* **2020**, *195*, 104795. https://doi.org/10.1016/j.catena.2020.104795.

(13) Liu, X.; Cheng, J.; Sprik, M.; Lu, X.; Wang, R. Understanding Surface Acidity of Gibbsite with First Principles Molecular Dynamics Simulations. *Geochim. Cosmochim. Acta* **2013**, *120*, 487–495. https://doi.org/10.1016/j.gca.2013.06.043.

(14) Yang, J.; Ge, M.; Jin, Q.; Chen, Z.; Guo, Z. Co-Transport of U(VI), Humic Acid and Colloidal Gibbsite in Water-Saturated Porous Media. *Chemosphere* **2019**, *231*, 405–414. https://doi.org/10.1016/j.chemosphere.2019.05.091.

(15) Harder, H. Clay Mineral Formation under Lateritic Weathering Conditions. *Clay Miner.* **1977**, *12* (4), 281–288. https://doi.org/10.1180/claymin.1977.012.4.01.

(16) Misra, C.; White, E. T. Crystallisation of Bayer Aluminium Trihydroxide. *J. Cryst. Growth* **1971**, *8* (2), 172–178. https://doi.org/10.1016/0022-0248(71)90138-2.

(17) Agnew, S. F.; Johnston, C. T. *Aluminum Solubility in Complex Electrolytes -13011*; 2013.

(18) Johnston, C. T.; Agnew, S. F.; Schoonover, J. R.; Kenney, J. W.; Page, B.; Osborn, J.; Corbin, R.

Raman Study of Aluminum Speciation in Simulated Alkaline Nuclear Waste. *Environ. Sci. Technol.* **2002**, *36* (11), 2451–2458. https://doi.org/10.1021/es011226k.

(19) Peterson, R. A.; Lumetta, G. J.; Rapko, B. M.; Poloski, A. P. Modeling of Boehmite Leaching from Actual Hanford High-Level Waste Samples. *Sep. Sci. Technol.* **2007**, *42* (8), 1719–1730. https://doi.org/10.1080/01496390701242111.

(20) Wells, B. E.; Knight, M. A.; Buck, E. C.; Daniel, R. C.; Meyer, P. A.; Tingey, J. M. *Estimate of Hanford Waste Insoluble Solid Particle Size and Density Distribution*; 2007.

(21) Gephart, R. E. A Short History of Waste Management at the Hanford Site. *Phys. Chem. Earth* **2010**, *35* (6–8), 298–306. https://doi.org/10.1016/j.pce.2010.03.032.

(22) Reynolds, J. G. The Apparent Solubility of Aluminum (III) in Hanford High-Level Waste. *J. Environ. Sci. Heal. - Part A Toxic/Hazardous Subst. Environ. Eng.* **2012**, *47* (14), 2213–2218. https://doi.org/10.1080/10934529.2012.707538.

(23) Peterson, R. A.; Buck, E. C.; Chun, J.; Daniel, R. C.; Herting, D. L.; Ilton, E. S.; Lumetta, G. J.; Clark, S. B. Review of the Scientific Understanding of Radioactive Waste at the U.S. DOE Hanford Site. *Environ. Sci. Technol.* **2018**, *52* (2), 381–396. https://doi.org/10.1021/acs.est.7b04077.

(24) Peeler, D. K.; Vienna, J. D.; Schweiger, M. J.; Fox, K. M. *Advanced High-Level Waste Glass Research and Development Plan*; 2015.

(25) Bénézeth, P.; Hilic, S.; Palmer, D. A. The Solubilities of Gibbsite and Bayerite Below 100 °C in Near Neutral to Basic Solutions. *J. Solution Chem.* **2016**, *45* (9), 1288–1302. https://doi.org/10.1007/s10953-016-0470-1.

(26) Königsberger, E.; May, P. M.; Hefter, G. Comprehensive Model of Synthetic Bayer Liquors. Part 3. Sodium Aluminate Solutions and the Solubility of Gibbsite and Boehmite. *Monatshefte fur Chemie* **2006**, *137* (9), 1139–1149. https://doi.org/10.1007/s00706-006-0526-9.

(27) Casassa, S.; Demichelis, R. Relative Energy of Aluminum Hydroxides: The Role of Electron Correlation. *J. Phys. Chem. C* **2012**, *116* (24), 13313–13321. https://doi.org/10.1021/jp300419t.

(28) Sipos, P. The Structure of Al(III) in Strongly Alkaline Aluminate Solutions - A Review. *J. Mol. Liq.*

652 **2009**, *146* (1–2), 1–14. https://doi.org/10.1016/j.molliq.2009.01.015.
653 (29) Shen, Z.; Kerisit, S. N.; Stack, A. G.; Rosso, K. M. Free-Energy Landscape of the Dissolution of
654 Gibbsite at High PH. *J. Phys. Chem. Lett.* **2018**, *9* (7), 1809–1814.
655 https://doi.org/10.1021/acs.jpclett.8b00484.
656 (30) Hu, J. Z.; Zhang, X.; Jaegers, N.; Wan, C.; Graham, T. R.; Hu, M. Y.; Pearce, C. I.; Felmy, A. R.;
657 Clark, S. B.; Rosso, K. M. Transitions in Al Coordination During Gibbsite Crystallization Using
658 High-Field ^{27} Al and ^{23} Na MAS NMR Spectroscopy. *J. Phys. Chem. C* **2017**, acs.jpcc.7b10424.
659 https://doi.org/10.1021/acs.jpcc.7b10424.
660 (31) Graham, T. R.; Dembowski, M.; Martinez-Baez, E.; Zhang, X.; Jaegers, N. R.; Hu, J.; Gruszkiewicz,
661 M. S.; Wang, H.-W. W.; Stack, A. G.; Bowden, M. E.; Delegard, C. H.; Schenter, G. K.; Clark, A.
662 E.; Clark, S. B.; Felmy, A. R.; Rosso, K. M.; Pearce, C. I. In Situ 27Al NMR Spectroscopy of
663 Aluminate in Sodium Hydroxide Solutions above and below Saturation with Respect to Gibbsite.
664 *Inorg. Chem.* **2018**, *57* (19), 11864–11873. https://doi.org/10.1021/acs.inorgchem.8b00617.
665 (32) Hetland, E. Electrolytic Conductivity of NaOH in H2O and of NaOD in D2O at 25°. A Vacuum
666 Distilling Apparatus for Deuterium Oxide. *J. Am. Chem. Soc.* **1946**, *68* (12), 2532–2535.
667 https://doi.org/10.1021/ja01216a030.
668 (33) Scheiner, S. Calculation of Isotope Effects from First Principles. *Biochim. Biophys. Acta - Bioenerg.*
669 **2000**, *1458* (1), 28–42. https://doi.org/10.1016/S0005-2728(00)00058-X.
670 (34) Zhou, X.; Wang, L.; Fan, X.; Wilfong, B.; Liou, S.-C.; Wang, Y.; Zheng, H.; Feng, Z.; Wang, C.;
671 Rodriguez, E. E. Isotope Effect between H 2 O and D 2 O in Hydrothermal Synthesis . *Chem.*
672 *Mater.* **2020**, *32* (2), 769–775. https://doi.org/10.1021/acs.chemmater.9b04121.
673 (35) Roskosz, M.; Deloule, E.; Ingrin, J.; Depecker, C.; Laporte, D.; Merkel, S.; Remusat, L.; Leroux,
674 H. Kinetic D/H Fractionation during Hydration and Dehydration of Silicate Glasses, Melts and
675 Nominally Anhydrous Minerals. *Geochim. Cosmochim. Acta* **2018**, *233*, 14–32.
676 https://doi.org/10.1016/j.gca.2018.04.027.
677 (36) Noonan, E. C. Solubility of Salts in Deuterium Oxide. *J. Am. Chem. Soc.* **1948**, *70*, 2915–2918.

(37) Enkelmann, D. D.; Hofmann, D. W. M.; Merz, K. Deuterium Shifts the Equilibrium: How Heavy Water Can Influence Organic Multicomponent Crystal Formation. *Cryst. Growth Des.* **2017**, *17* (9), 4726–4729. https://doi.org/10.1021/acs.cgd.7b00654.

(38) Loh, J. S. C.; Fogg, A. M.; Watling, H. R.; Parkinsona, G. M. A Kinetic Investigation of Gibbsite Precipitation Using in Situ Time Resolved Energy Dispersive X-Ray Diffraction. *Phys. Chem. Chem. Phys.* **2000**, *2*, 3597–3604. https://doi.org/10.1039/b003050n.

(39) Loh, J. S. C.; Watling, H. R.; Parkinson, G. M. The Effect of Isotopic Substitution of Deuterium for Hydrogen on the Morphology of Products Precipitated from Synthetic Bayer Solutions. *J. Cryst. Growth* **2002**, *237–239* (1–4), 2178–2182. https://doi.org/10.1016/S0022-0248(01)02265-5.

(40) Fenby, D. V.; Kooner, Z. S.; Khurma, J. R. Deuterium Isotope Effects in Liquid—Liquid Phase Diagrams: A Review. *Fluid Phase Equilib.* **1981**, *7* (3–4), 327–338. https://doi.org/10.1016/0378-3812(81)80015-5.

(41) McDougall, A. O.; Long, F. A. Relative Hydrogen Bonding of Deuterium. II. Acid Ionization Constants in H2O And D2O. *J. Am. Chem. Soc* **1962**, *66*, 429–433.

(42) Zhang, X.; Zhang, X.; Graham, T. R.; Pearce, C. I.; Mehdi, B. L.; N'Diaye, A. T.; Kerisit, S.; Browning, N. D.; Clark, S. B.; Rosso, K. M. Fast Synthesis of Gibbsite Nanoplates and Process Optimization Using Box-Behnken Experimental Design. *Cryst. Growth Des.* **2017**, *17* (12), 6801–6808. https://doi.org/10.1021/acs.cgd.7b01400.

(43) Van Geet, A. L. Calibration of Methanol Nuclear Magnetic Resonance Thermometer at Low Temperature. *Anal. Chem.* **1970**, *42* (6), 679–680. https://doi.org/10.1021/ac60288a022.

(44) Callaghan, P. T.; Le Gros, M. A.; Pinder, D. N. The Measurement of Diffusion Using Deuterium Pulsed Field Gradient Nuclear Magnetic Resonance. *J. Chem. Phys.* **1983**, *79* (12), 6372–6381. https://doi.org/10.1063/1.445745.

(45) Stejskal, E. O.; Tanner, J. E. Spin Diffusion Measurements: Spin Echoes in the Presence of a Time-Dependent Field Gradient. *J. Chem. Phys.* **1965**, *42* (1), 288–292. https://doi.org/10.1063/1.1695690.

(46) Tanner, J. E. Pulsed Field Gradients for NMR Spin-Echo Diffusion Measurements. *Rev. Sci. Instrum.* **1965**, *36* (8), 1086–1087. https://doi.org/10.1063/1.1719808.

(47) Wesolowski, D. J. Aluminum Speciation and Equilibria in Aqueous Solution: I. The Solubility of Gibbsite in the System Na-K-Cl-OH-Al(OH)4 from 0 to 100°C. *Geochim. Cosmochim. Acta* **1992**, *56* (3), 1065–1091. https://doi.org/10.1016/0016-7037(92)90047-M.

(48) Sipos, P.; Hefter, G.; May, P. M. 27Al NMR and Raman Spectroscopic Studies of Alkaline Aluminate Solutions with Extremely High Caustic Content - Does the Octahedral Species Al(OH)63- Exist in Solution? *Talanta* **2006**, *70* (4), 761–765. https://doi.org/10.1016/j.talanta.2006.02.008.

(49) Megyes, T.; Bálint, S.; Grósz, T.; Radnai, T.; Bakó, I.; Sipos, P. The Structure of Aqueous Sodium Hydroxide Solutions: A Combined Solution x-Ray Diffraction and Simulation Study. *J. Chem. Phys.* **2008**, *128* (4). https://doi.org/10.1063/1.2821956.

(50) Millet, O.; Loria, J. P.; Kroenke, C. D.; Pons, M.; Palmer, A. G. The Static Magnetic Field Dependence of Chemical Exchange Linebroadening Defines the NMR Chemical Shift Time Scale. *J. Am. Chem. Soc.* **2000**, *122* (12), 2867–2877. https://doi.org/10.1021/ja993511y.

(51) Nortier, P.; Chagnon, P.; Lewis, A. E. Modelling the Solubility in Bayer Liquors: A Critical Review and New Models. *Chem. Eng. Sci.* **2011**, *66* (12), 2596–2605. https://doi.org/10.1016/j.ces.2011.03.004.

(52) Jancso, G.; Van Hook, W. A. Condensed Phase Isotope Effects. *Chem. Rev.* **1974**.

(53) Cross, P. C.; Burnham, J.; Leighton, P. A. The Raman Spectrum and the Structure of Water. *J. Am. Chem. Soc.* **1937**, *59* (6), 1134–1147. https://doi.org/10.1021/ja01285a052.

(54) Moolenaar, R. J.; Evans, J. C.; Mckeever, L. D. The Structure of the Aluminate Ion in Solutions at High PH. *J. Phys. Chem.* **1969**, *74* (20), 3629–3636. https://doi.org/10.1021/j100714a014.

(55) Dembowski, M.; Snyder, M. M.; Delegard, C. H.; Reynolds, J. G.; Graham, T. R.; Wang, H.-W.; Leavy, I. I.; Baum, S. R.; Qafoku, O.; Fountain, M. S.; Rosso, K. M.; Clark, S. B.; Pearce, C. I. Ion–Ion Interactions Enhance Aluminum Solubility in Alkaline Suspensions of Nano-Gibbsite (α-

730 Al(OH) 3) with Sodium Nitrite/Nitrate . *Phys. Chem. Chem. Phys.* **2020**.
731 https://doi.org/10.1039/c9cp05856g.
732 (56) Graham, T. R.; Semrouni, D.; Mamontov, E.; Ramirez-Cuesta, A. J.; Page, K.; Clark, A.; Schenter,
733 G. K.; Pearce, C. I.; Stack, A. G.; Wang, H. W. Coupled Multimodal Dynamics of Hydrogen-
734 Containing Ion Networks in Water-Deficient, Sodium Hydroxide-Aluminate Solutions. *J. Phys.*
735 *Chem. B* **2018**, *122* (50), 12097–12106. https://doi.org/10.1021/acs.jpcb.8b09375.
736 (57) Wang, H. W.; Graham, T. R.; Mamontov, E.; Page, K.; Stack, A. G.; Pearce, C. I. Countercations
737 Control Local Specific Bonding Interactions and Nucleation Mechanisms in Concentrated Water-
738 in-Salt Solutions. *J. Phys. Chem. Lett.* **2019**, *10* (12), 3318–3325.
739 https://doi.org/10.1021/acs.jpclett.9b01416.
740 (58) Wimpenny, J.; Colla, C. A.; Yu, P.; Yin, Q. Z.; Rustad, J. R.; Casey, W. H. Lithium Isotope
741 Fractionation during Uptake by Gibbsite. *Geochim. Cosmochim. Acta* **2015**, *168*, 133–150.
742 https://doi.org/10.1016/j.gca.2015.07.011.
743 (59) Engel, T.; Reid, P. *Thermodynamics, Statistical Thermodynamics, and Kinetics*, 3rd ed.; 2013.
744 (60) Wesolowski, D. J.; Palmer, D. A. Aluminum Speciation and Equilibria in Aqueous Solution: V.
745 Gibbsite Solubility at 50??C and PH 3-9 in 0.1 Molal NaCl Solutions (a General Model for
746 Aluminum Speciation; Analytical Methods). *Geochim. Cosmochim. Acta* **1994**, *58* (14), 2947–2969.
747 https://doi.org/10.1016/0016-7037(94)90171-6.
748